THE JOURNAL OF PHYSICAL CHEMISTRY Letters

Biophysical Chemistry, Biomolecules, and Biomaterials; Surfactants and Membranes

Fusion Pores Live on the Edge

Edgar M. Blokhuis, Massimo D'agostino, Andreas Mayer, and Herre Jelger Risselada

J. Phys. Chem. Lett., **Just Accepted Manuscript** • DOI: 10.1021/acs.jpclett.9b03563 • Publication Date (Web): 16 Jan 2020

Fusion pores live on the edge[†]

Edgar M. Blokhuis,[‡] D'Agostino Massimo,[¶] Andreas Mayer,[§] and H. Jelger Risselada[*,‡,‖]

‡*Leiden University, Leiden Institute of Chemistry (LIC), The Netherlands*

¶*Department of Molecular Medicine and Medical Biotechnology, University of Naples Federico II, Naples, Italy*

§*Département de Biochimie, Université de Lausanne, Epalinges, Switzerland*

‖*Georg-August University of Goettingen, Dept. of Theoretical Physics, Germany*

E-mail: hrissel@gwdg.de

Phone: +49 551 39 5995. Fax: +49 551 39 9631

Abstract

Biological transmission of vesicular content occurs by opening of a fusion pore. Recent experimental observations have illustrated that fusion pores between vesicles that are docked by an extended flat contact zone are located at the edge (vertex) of this zone. We modeled this experimentally observed scenario by coarse-grained molecular simulations and elastic theory. This revealed that fusion pores experience a direct attraction toward the vertex. The size adopted by the resulting vertex pore strongly depends on the apparent contact angle between the adhered vesicles even in the absence of membrane surface tension. Larger contact angles substantially increase the equilibrium size of the vertex pore. Since the cellular membrane fusion machinery actively docks membranes, it facilitates a collective expansion of the contact zone and

[†]A footnote for the title

increases the contact angle. In this way, the fusion machinery can drive expansion of the fusion pore by free energy equivalents of multiple tens of k_BT from a distance, and not only through the fusion proteins that reside within the fusion pore.

Biological membrane fusion proceeds via the opening of a fusion pore to release vesicular cargoes that are vital for many biological processes, including exocytosis, intracellular trafficking, fertilization, and viral entry. Electron cryo-tomography (cryo-ET) observations of *in vivo* fusion events in synapses[1] and yeast cells[2] suggest that fusion is preceded by close apposition of the two membranes, which for larger vesicles (> 100 nm) results in the formation of an extended flat contact or docking zone.[3] Subsequent fusion is thought to occur at the highly curved membrane perimeter of the contact zone – the vertex.[3,4] Indeed, cryo-ET of reconstituted mitochondrial fusion as well as fluorescence microscopy studies of yeast vacuole fusion revealed fusion pores that are located at the vertex, see ref.[2,5] and Fig. 1.

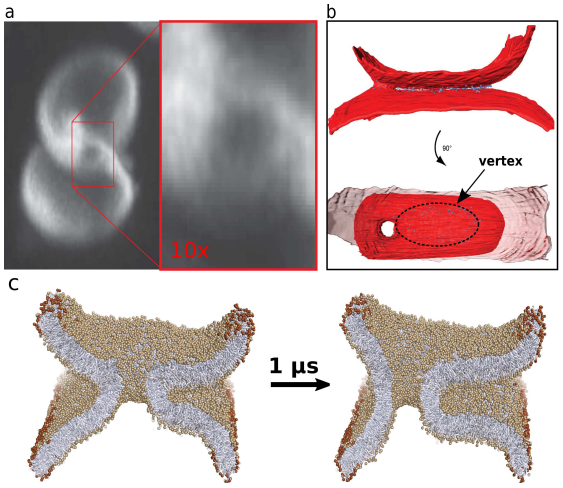

Figure 1: Vertex fusion pores in membrane fusion. (a) Stacked tomography imaging of the in-vivo fusion reaction between two yeast vacuoles (adapted from[2]). (b) Cryo-electron tomography of the adhesion zone formed in reconstituted mitochondrial fusion (adapted from[5]). (c) A centrally located pore formed between two curved lipid membrane sheets undergoes spontaneous symmetry breaking in a coarse-grained molecular dynamics simulation (see supplementary movie). The dark brown colored beads indicate immobilized beads, which spatially constrain the free membrane ends (see *SI* and Fig. S4)

Pores are intrinsically attracted toward the vertex. The physical principle underlying 'vertex pores' can be illustrated from a coarse-grained molecular simulation of two curved

membrane sheets, which are being connected by a centrally located fusion pore (see *SI* for details). Rather than symmetrizing membrane curvature at both sides of the pore, such a system 'escapes' into a highly asymmetric shape by adopting an off-centered location – a vertex pore (see Fig. 1c). Attraction toward the edge is in our example explained by a strong, favorable reduction in membrane curvature at the left side of the pore, whereas the curvature at the opposing side remains rather conserved. Symmetry breaking, i.e. location near the edge, thus provides a net free energy gain. A fusion pore – if not being nucleated at the vertex – will thus become captured at the vertex after having diffused to this location. However, quite in contrast to the stereotypical model of an axial symmetric fusion pore, a 'vertex pore' is not characterized by axial symmetry because of the varying membrane curvature along its circumference. The consequences of such an altered architecture/symmetry on pore size have remained unexplored.

A large amount of both theoretical work (e.g., continuum elastic models and molecular simulations),[6–15] and experimental observations (e.g., patch-clamp experiments and Cryo-EM tomography)[2,5,16–19] have substantially advanced our understanding of the structure, composition, location, dynamics and energetics of fusion pores. Irrespective of their topology, fusion pores in living cells are likely to be neither protein channels nor purely lipid, but are probably proteo-lipidic hybrid structures.[16–19] Fusion proteins such as SNAREs and associated tether complexes are integrated into them and play an active role in the opening and dynamics of the fusion pore via steric, entropic and electrostatic forces.[19–22] An expansive radial force on the pore originates from the crowding of proteins at the pores circumference. The proteins must be part of the pore (a proteolipidic pore) in order to influence pore size in this way. The architecture/structure of a vertex pore *additionally* depends on the (effective) contact angle at the contact zone (Fig. 2). Here, we will illustrate that this contact angle determines the equilibrium size of the vertex pore. The important consequence of this principle is that docking mediators such as Mitofusins, SNAREs and associated tether

complexes, which determine the size of the contact zone and hence the contact angle, can influence fusion pore dynamics not only when being directly integrated into the pore, but they can also impose an additional distal influence on the pore.

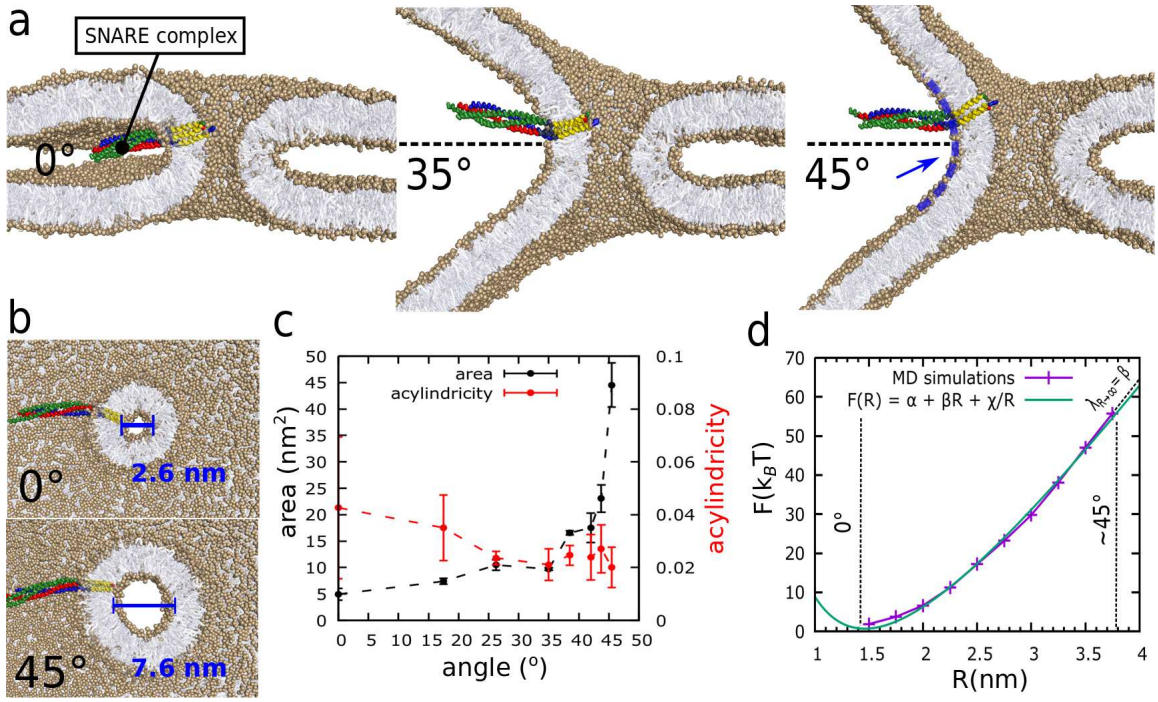

Figure 2: Molecular dynamics simulations of the vertex fusion pore under different contact angles. The depicted SNARE complex indicates the length scale. (a) Final states of the system (after 2 μs) under effective contact angles of 0°, 35°, and 45°. The blue dashed line indicates the induced axial asymmetry of the pore's circumference. (b) Corresponding top-view of the fusion pore. (c) Area and Acylindricity ($\in [0, 1]$) of the fusion pore as a function of contact angle. Acylindricity values close to zero indicate that the pore adopts a perfect circular shape. The error bars are the (statistically independent) standard errors derived by ensemble block averaging. (d) Free energy cost associated with the radial expansion of a free, symmetric pore ($\theta = 0°$). Adopting a pore area of 45 nm^2 (a radius of $\simeq$ 3.8 nm), i.e. the native pore size at $\theta = 45°$, requires a free energy equivalent of about 55 k_BT. The shape of $F(R)$ is qualitatively described by the function, $F(R) = \alpha + \beta R + \frac{\gamma}{R}$.

Vertex attractions inherently facilitate pore expansion. Since it is virtually impossible to experimentally discern the intrinsic contribution of the contact angle from a potentially present membrane tension, we reconstructed a coarse-grained molecular simulation model of an edge fusion pore located at the perimeter of an extended docking zone (see Fig 2a). Tension-less membrane conditions were ensured by breaking the periodicity along the x-

dimension; which enables the membranes to freely adopt area. To study a specific effective contact angle θ, we employed an external field to enforce the membranes to adopt a desired angle with respect to the contact zone (see SI for technical details). In this procedure, we started from a system comprised of two flat membranes where a small stable fusion pore (area of $\sim$5 nm^2) is already present. Then, we gradually increased the contact angle. From this trajectory we extracted different contact angles which we independently studied by a long equilibrium run (2 μs) at constant contact angle. Fig. 2b, c shows the equilibrium size of the fusion pore as a function of contact angle. Surprisingly, at $\theta > 30°$ the area of the meta-stable pore steeply increases up to 9-fold in size (5 nm^2 $\rightarrow$ 45 nm^2) at $\theta = 45°$. Conveniently, the free energy F required to expand a symmetric fusion pore ($\theta = 0°$) to a radius R can be extracted from our molecular simulations by enforcing a radial expansion of the pore via an applied external field, and extracting the average, responsive force, $\frac{dF}{dR}$, acting against that field (see Fig. 2d). Intriguingly, a 9-fold expansion of a symmetric fusion pore ($\theta = 0°$) would require a free energy equivalent of more than 50 $k_\mathrm{B}T$. Thus, the vertex provides a substantial driving force for pore expansion. Alternatively, pore size may be enhanced by binding of a voluminous protein complex such as, e.g., the HOPS complex near the fusion pore.[23] Within such a scenario expansion occurs when the effective spherical size of a nearby complex is above a size of $\sim$ 20 nm (Fig. S9), which can be attained by common SNARE-associated protein complexes.[24,25]

Thermodynamic description of a fusion pore. A fusion pore adopts a thermodynamically stable size because of a force balance along its circumference, $2\pi R$. The free energy of the axially symmetric fusion pore can be expanded in terms of R as: $F(R) = \alpha + \beta R + \frac{\gamma}{R} + \frac{\delta}{R^2}$ ... ($R > 0$). Constant terms within the free energy (α) can be omitted. This expansion directly follows from the fact that the contribution of one of its principle radii to the free energy must vanish when the pore becomes large. In that regime, $F(R)$ linearly increases with the length of the interface, $F(R) \propto R$ ($R \gg 0$) because the line tension, being thermodynamically

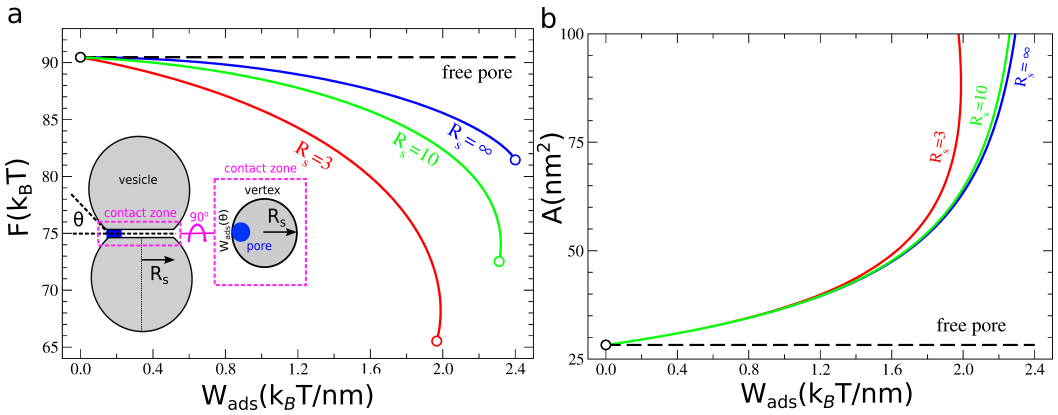

Figure 3: Vertex attractions drive pore expansion. (a) Free energy of the vertex pore as a function of edge attractions. (b) The corresponding equilibrium area of the pore. The dashed black line ('free pore') illustrates the value of a common fusion pore (no vertex attractions). The size of the contact zone is in reduced units: $R_s = 3$ (12.7 nm) and $R_s = 10$ (42.4 nm).

defined as $\lambda_R = \frac{1}{2\pi}\frac{dF}{dR}$, becomes constant, therefore $\lambda_{R\to\infty} = \frac{\beta}{2\pi}$. The competition between the *contractive* linear term ($\lambda_{R\to\infty}$) and the *expansive* rigidity term(s) gives rise to a force balance: A free energy minimum which determines the equilibrium size of the pore. In regular membrane pores where the contractive forces is dominant such a free energy minimum is extremely shallow and pores are either unstable or short-lived.[26] Fig. 2d illustrates that inclusion of the first 'rigidity' term ($\frac{\gamma}{R}$) suffices to qualitatively describe the free energy associated with fusion pore expansion. This justifies the thermodynamic description of a three-dimensional fusion pore by an enclosed contour (a two-dimensional vesicle) whose size and shape is understood from a balance between the contractive force, $\lambda_{R\to\infty,\theta=0}$, and the bending rigidity, $\kappa_{2D} = \frac{\gamma}{2\pi}$ (see *SI*).

Why vertex attractions impose expansion. Since a larger contact angle enables the vertex pore to relax its curvature stress at least on one side, it translates into a stronger vertex-attraction. This attraction is effectively modeled by the force, W_{ads}. Vertex pore formation is analogous to the adhesion of a 2-dimensional vesicle (the pore) to a curved substrate (the vertex).[14,27,28] The shape equations corresponding to this variational wetting problem were solved numerically (see *SI*). Fig. 3 illustrates that edge attractions push the force balance

towards larger pore sizes, in correspondence with the molecular simulations. The vertex attraction W_{ads} *locally* compensates for the intrinsic contractive force acting on the pore's circumference, being $\lambda_{R\to\infty,\theta=0}$. Evidently, even a local, asymmetric release of bending energy already suffices to expand the pore. By consequence, axially symmetric fusion pores are expected to expand when the distance between the two opposed membranes increases, because of a global, symmetric release in bending energy.[7] Decreasing the radius of the vertex R_s below a microscopic size – thereby better matching the pore's native circular shape – further increases pore growth. This suggests that the expected pore growth is stronger in smaller vesicles, such as SUVs and synaptic vesicles, because of a smaller contact zone, given that the (apparent) contact angle between the adhered vesicles is similar. Finally, modeling the vertex as an attractive hard wall induces deformation of the pore when interacting with the vertex (see *SI*). The observation of a circular pore in the molecular simulations therefore rather indicates that vertex interactions are soft.

Vertex pores in vivo. A remaining question is whether vertex attractions also significantly affect pore expansion *in vivo*, for which we should expect contact angles $\theta > 30°$. Based on the microscopic observation of docked yeast vacuoles,[2] we estimated a contact angle of about 50° (see Fig. S10). However, it is challenging to directly relate the microscopically observed contact angle in experiments with the here-reported nanoscopic, apparent contact angle.[29] Fortunately, these nanoscopic contact angles are directly transferable into a concomitant adhesion free energy per unit area (a surface tension), σ, via the relationship $\sigma_\theta = \frac{\kappa}{2R_\theta^2}$,[29] with κ being the bending modulus ($\sim 20\ k_{\mathrm{B}}T$) and R_θ the radius of adhesion – the membrane curvature (radius) at the point of intersection with the contact zone (see Fig S11 and S12). We find $R_{\theta=35} \sim 80$ nm $\rightarrow \sigma_{\theta=35} = 1.6 \times 10^{-3}\ k_{\mathrm{B}}T/\mathrm{nm}^2$ and $R_{\theta=45} \sim 40$ nm $\rightarrow \sigma_{\theta=45} = 5.8 \times 10^{-3}\ k_{\mathrm{B}}T/\mathrm{nm}^2$. Thus, we predict that the protein-mediated adhesion/docking of membranes must yield $1.6 \times 10^{-3}\ k_{\mathrm{B}}T/\mathrm{nm}^2$ or 6.6×10^{-3} mN/m ($1\ k_{\mathrm{B}}T/\mathrm{nm}^2 = 4.114$ mN/m at 293K) to substantially contribute to the free energy of the fusion pore via vertex in-

teractions. This value represents a common adhesive interaction between lipid membranes[30] and can be experimentally determined via micropipette aspiration.[30,31] Since the direct contribution of this adhesive interaction to the pore's free energy is approximately, σA,[7,12] its intrinsic effect on equilibrium pore size is small ($< 1\ k_{\mathrm{B}}T$).

A compelling amount of evidence suggests that fusion proteins actively contribute to the expansion of a formed fusion pore.[19–22] Such a pore expansion can be driven by entropic repulsions between fusion proteins integrated within the pore.[20] As shown here, vertex attractions offer an additional and perhaps surprising mechanism, by which also distal fusion proteins can substantially contribute to the expansion of the fusion pore via a collective expansion of the contact zone. Furthermore, our work strongly suggests that the 'black holes' recently observed in yeast vacuole fusion assays, i.e. sub-nanometer sized fusion pores that are too small to allow passage of soluble dye molecules, are not explained by their observed vertex location.[2] Since vertex attractions are rather expected to increase the size of a fusion pore, 'black holes' must be due to the presence of an additional, dominant contractive force on the fusion pore in docked yeast vacuoles. For example, the presence of electrostatic attractions between net charged lipid species, protein residues and ions inside the pore.[16] Finally, popular experimental assays for studying the conductance of the fusion pore are based on the fusion reaction between nanodiscs and membranes.[32] Nanodiscs are comprised of a peptide or polymer capped free membrane edge that introduces a spatially heterogeneous membrane environment analogous to the vertex of the docking zone. Therefore, the free energy of the fusion pore may dependent on its location within the disc. Since 'edge attractions' increase pore size regardless of the edge's structural nature (Fig. 3), it is a relevant question whether the fusion pore formed in larger nano discs (> 20 nm) preferably locates near the rim (edge attraction) or whether it adopts a central location (edge repulsion).

Acknowledgement

HJR acknowledges the Life@nano excellence initiative (state of Lower Saxony) and the NWO Vidi scheme for funding. AM has been supported by the SNSF (31003A_179306). The HLRN Berlin/Hannover & NWO SURFsara (the netherlands) are acknowledged for computational resources.

Supporting Information Available

The SI provides additional simulations and calculations. The supplementary movie shows how a centrally located fusion pore breaks it symmetry.

References

(1) Imig, C.; Min, S.-W.; Krinner, S.; Arancillo, M.; Rosenmund, C.; Südhof, T. C.; Rhee, J.; Brose, N.; Cooper, B. H. The Morphological and Molecular Nature of Synaptic Vesicle Priming at Presynaptic Active Zones. *Neuron* **2014**, *84*, 416–431.

(2) D'Agostino, M.; Risselada, H. J.; Endter, L. J.; Comte-Miserez, V.; Mayer, A. SNARE-mediated membrane fusion arrests at pore expansion to regulate the volume of an organelle. *The EMBO Journal* **2018**, e99193.

(3) Hernandez, J. M.; Stein, A.; Behrmann, E.; Riedel, D.; Cypionka, A.; Farsi, Z.; Walla, P. J.; Raunser, S.; Jahn, R. Membrane Fusion Intermediates via Directional and Full Assembly of the SNARE Complex. *Science* **2012**, *336*, 1581–1584.

(4) Wang, L.; Seeley, E.; Wickner, W.; Merz, A. J. Vacuole Fusion at a Ring of Vertex Docking Sites Leaves Membrane Fragments within the Organelle. *Cell* **2002**, *108*, 357–369.

(5) Brandt, T.; Cavellini, L.; Kühlbrandt, W.; Cohen, M. M. A mitofusin-dependent docking ring complex triggers mitochondrial fusion in vitro. *eLife* **2016**, *5*.

(6) Nanavati, C.; Markin, V.; Oberhauser, A.; Fernandez, J. The exocytotic fusion pore modeled as a lipidic pore. *Biophys. J.* **1992**, *63*, 1118–1132.

(7) Chizmadzhev, Y.; Cohen, F.; Shcherbakov, A.; Zimmerberg, J. Membrane mechanics can account for fusion pore dilation in stages. *Biophys. J.* **1995**, *69*, 2489–2500.

(8) Jackson, M. Minimum Membrane Bending Energies of Fusion Pores. *J. Mem. Biol.* **2009**, *231*, 101–115.

(9) Grafmüller, A.; Shillcock, J.; Lipowsky, R. The Fusion of Membranes and Vesicles: Pathway and Energy Barriers from Dissipative Particle Dynamics. *Biophys. J.* **2009**, *96*, 2658–2675.

(10) Yoo, J.; Jackson, M. B.; Cui, Q. A Comparison of Coarse-Grained and Continuum Models for Membrane Bending in Lipid Bilayer Fusion Pores. *Biophys. J.* **2013**, *104*, 841–852.

(11) Ryham, R. J.; Ward, M. A.; Cohen, F. S. Teardrop shapes minimize bending energy of fusion pores connecting planar bilayers. *Phys. Rev. E* **2013**, *88*.

(12) Long, R.; Hui, C.-Y.; Jagota, A.; Bykhovskaia, M. Adhesion energy can regulate vesicle fusion and stabilize partially fused states. *J R Soc Interface* **2012**, *9*, 1555–1567.

(13) Gao, L.; Lipowsky, R.; Shillcock, J. Tension-induced vesicle fusion: pathways and pore dynamics. *Soft Matter* **2008**, *4*, 1208–1214.

(14) Risselada, H. J.; Smirnova, Y.; Grubmüller, H. Free Energy Landscape of Rim-Pore Expansion in Membrane Fusion. *Biophys. J.* **2014**, *107*, 2287–2295.

(15) Sharma, S.; Lindau, M. Molecular mechanism of fusion pore formation driven by the neuronal SNARE complex. *Proc. Natl. Aca. Sci. U.S.A* **2018**, *115*, 12751–12756.

(16) Han, X.; Wang, C. T.; Bai, J.; Chapman, E. R.; Jackson, M. B. Transmembrane Segments of Syntaxin Line the Fusion Pore of $Ca2^{+}$-Triggered Exocytosis. *Science* **2004**, *304*, 289–292.

(17) Fang, Q.; Berberian, L. W., K. Gong; Hafez, I.; Sørensen, J. B.; Lindau, M. The role of the C terminus of the SNARE protein SNAP-25 in fusion pore opening and a model for fusion pore mechanics. *Proc. Natl. Aca. Sci. U.S.A* **2008**, *105*, 15388–15392.

(18) Bao, H.; Goldschen-Ohm, M.; Jeggle, P.; Chanda, B.; Edwardson, J. M.; Chapman, E. R. Exocytotic fusion pores are composed of both lipids and proteins. *Nature Structural & Molecular Biology* **2015**, *23*, 67–73.

(19) Bao, H.; Das, D.; Courtney, N. A.; Jiang, Y.; Briguglio, J. S.; Lou, X.; Roston, D.; Cui, Q.; Chanda, B.; Chapman, E. R. Dynamics and number of trans-SNARE complexes determine nascent fusion pore properties. *Nature* **2018**, *554*, 260–263.

(20) Wu, Z.; Thiyagarajan, S.; O'Shaughnessy, B.; Karatekin, E. Regulation of Exocytotic Fusion Pores by SNARE Protein Transmembrane Domains. *Frontiers in Molecular Neuroscience* **2017**, *10*.

(21) Wu, Z.; Bello, O. D.; Thiyagarajan, S.; Auclair, S. M.; Vennekate, W.; Krishnakumar, S. S.; O'Shaughnessy, B.; Karatekin, E. Dilation of fusion pores by crowding of SNARE proteins. *eLife* **2017**, *6*.

(22) Mostafavi, H.; Thiyagarajan, S.; Stratton, B. S.; Karatekin, E.; Warner, J. M.; Rothman, J. E.; O'Shaughnessy, B. Entropic forces drive self-organization and membrane fusion by SNARE proteins. *Proc. Natl. Aca. Sci. U.S.A* **2017**, *114*, 5455–5460.

(23) D'Agostino, M.; Risselada, H. J.; Lürick, A.; Ungermann, C.; Mayer, A. A tethering complex drives the terminal stage of SNARE-dependent membrane fusion. *Nature* **2017**,

(24) Brocker, C.; Kuhlee, A.; Gatsogiannis, C.; kleine Balderhaar, H. J.; Honscher, C.; Engelbrecht-Vandre, S.; Ungermann, C.; Raunser, S. Molecular architecture of the multisubunit homotypic fusion and vacuole protein sorting (HOPS) tethering complex. *Proc. Natl. Aca. Sci. U.S.A* **2012**, *109*, 1991–1996.

(25) Chou, H.-T.; Dukovski, D.; Chambers, M. G.; Reinisch, K. M.; Walz, T. CATCHR, HOPS and CORVET tethering complexes share a similar architecture. *Nat. Struct. Mol. Biol.* **2016**, *23*, 761–763.

(26) Ting, C. L.; Awasthi, N.; Muller, M.; Hub, J. S. Metastable Prepores in Tension-Free Lipid Bilayers. *Phys. Rev. Lett* **2018**, *120*.

(27) Seifert, U. Adhesion of vesicles in two dimensions. *Phys. Rev. A* **1991**, *43*, 6803–6814.

(28) Shi, W.; Feng, X. Q.; Gao, H. Two-dimensional model of vesicle adhesion on curved substrates. *Acta Mech. Sinica* **2006**, 529–535.

(29) Seifert, U.; Lipowsky, R. Adhesion of vesicles. *Phys. Rev. A* **1990**, *42*, 4768–4771.

(30) Sun, Y.; Lee, C.-C.; Huang, H. W. Adhesion and Merging of Lipid Bilayers: A Method for Measuring the Free Energy of Adhesion and Hemifusion. *Biophys. J.* **2011**, *100*, 987–995.

(31) Warner, J. M.; Karatekin, E.; O'Shaughnessy, B. Model of SNARE-Mediated Membrane Adhesion Kinetics. *PLoS ONE* **2009**, *4*, e6375.

(32) Karatekin, E. Toward a unified picture of the exocytotic fusion pore. *FEBS Letters* **2018**, *592*, 3563–3585.